Letter

# Imprints of $\alpha$ clustering in the density profiles of $^{12}$C and $^{16}$O

W. Horiuchi [1,2,3,4,*] and N. Itagaki [1,2,†]

[1]*Department of Physics, Osaka Metropolitan University, Osaka 558-8585, Japan*
[2]*Nambu Yoichiro Institute of Theoretical and Experimental Physics (NITEP), Osaka Metropolitan University, Osaka 558-8585, Japan*
[3]*RIKEN Nishina Center, Wako 351-0198, Japan*
[4]*Department of Physics, Hokkaido University, Sapporo 060-0810, Japan*

(Received 11 October 2022; accepted 1 February 2023; published 21 February 2023)

The $^4$He nucleus is a well bound and highly correlated four-nucleon system that is also found in the form of $\alpha$ clusters as a substructure in nuclear many-body systems. The standard single-particle shell model cannot represent these four-body correlations. It is highly desirable to find a simple way to identify and distinguish these fundamental structures without large-scale computations. In this paper, we investigate with intrinsic Slater determinants as trial states in how far these two competing pictures prevail in the ground states of $^{12}$C and $^{16}$O. The trial states can describe both the $j$-$j$ coupling shell-model and $\alpha$-cluster configurations in a unified way. One-body density distributions of the trial states are calculated and compared to elastic scattering cross section data. The parameters of the trial state are chosen to reproduce the experimental charge radii. A well developed cluster structure is characterized by an enhancement of the differential elastic scattering cross sections, as well as the elastic charge form factors around the first peak positions. The density profiles of the internal regions can also be probed at higher momentum transfer regions beyond the second minimum. With these trial states one can visualize the competition between cluster and shell structure in an intuitive and simple way.

DOI: 10.1103/PhysRevC.107.L021304

How we can distinguish shell and cluster states quantitatively is a fundamental question of nuclear structure physics. Each nucleus is composed of protons and neutrons. In the single-particle shell model, they are considered to perform independent particle motions in a self-consistent potential [1]. On the other hand, two protons and two neutrons often form an $\alpha$ cluster as the binding energy of $^4$He is so large compared to the neighboring nuclei. These two different aspects, the cluster and shell picture, compete in the nuclear structure [2].

From the point of view of the nucleon-nucleon interaction, the noncentral interactions, the spin-orbit and tensor interactions, play significant roles in the nuclear systems, which are the key ingredients for this competition. The spin-orbit interaction is a driving force that stabilizes the shell-model picture (the magic number can be explained owing to this effect) and break $\alpha$ clusters [3], whereas the strong binding of $^4$He comes from the tensor contribution which stabilizes the $\alpha$-cluster structure [4]. The balance of these noncentral interactions governs the competition of the two pictures [5].

For $^{12}$C and $^{16}$O, there have been numerous works based on the three- and four-$\alpha$ cluster models, respectively [6–10]. However, from the shell-model point of view, these nuclei correspond to the closures of $p_{3/2}$ and $p_{1/2}$ subshells, respectively. In $^{12}$C, the attractive effect of the spin-orbit interaction breaks the $\alpha$ clusters according to the shell-model picture, but the $\alpha$ cluster model succeeded in explaining various electromagnetic properties. An *ab initio* computation was carried out to solve this 12-nucleon problem and succeeded in reproducing the elastic charge form factor of $^{12}$C [11]. The recent *ab initio* shell-model calculation showed the mixing of the shell and cluster configurations [12], as suggested by molecular dynamics calculations [13,14]. For $^{16}$O, if we take a small distance between four $\alpha$ clusters with a tetrahedron configuration, the wave function agrees with the shell model. In contrast, recent *ab initio* calculations suggested the possibility of four-$\alpha$ clusters with finite relative distance for the ground state [15].

It is highly desirable to have a simple picture in order to estimate if $\alpha$-cluster or shell-model structure dominates nuclear states as it impacts the astrophysically important reaction rates, e.g., triple-$\alpha$ reactions involving the so-called Hoyle state [16,17]. For this purpose, the basis states of the antisymmetrized quasicluster model (AQCM) [18–31] are quite helpful as they provide an ansatz for a simple trial state that is capable of representing both shell-model and cluster states on the same footing.

In the following, we choose the parameters of these states such that they represent either a pure $\alpha$ cluster, a single-particle shell-model state, or something in between. As there is no Hamiltonian or eigenvalue problem involved, nor a Ritz variational method to find optimal parameters, we require instead that each trial state reproduces the experimental charge radius. This is possible by adjusting the spatial parameters of the two states as explained in detail below. In this way, any ambiguities coming from a model Hamiltonian or the choice of a many-body Hilbert space are ruled out.

*whoriuchi@omu.ac.jp
†itagaki@omu.ac.jp

 

The one-body density of each trial state reproducing the experimental charge radius is used to calculate the proton-nucleus elastic scattering cross section and the elastic charge form factor, which are then compared to measured data. This procedure allows to judge which trial state gives a better description of the data and hence which picture is closer to nature.

The shell and cluster trial states are represented based on the $N\alpha$ cluster model [2] and its extension: the AQCM [18–31]. The trial state is fully antisymmetrized ($\mathcal{A}$) and is expressed by the product of the $\alpha$ particle wave functions, $\Phi_\alpha$, as

$$\Phi(\nu, d, \Lambda) = \mathcal{A}\left\{\prod_{i=1}^{N} \Phi_\alpha(\nu, R_i, \Lambda)\right\}. \tag{1}$$

Note that the inter-$\alpha$-cluster distance is defined by $d = |\boldsymbol{R}_i - \boldsymbol{R}_j|$ $(i \neq j)$, where the three $\alpha$'s ($^{12}$C) and four $\alpha$'s ($^{16}$O) are placed with equilateral triangular and tetrahedron shapes, respectively. The wave function of the $i$th $\alpha$ particle with the Gaussian center parameter $\boldsymbol{R}_i$, is defined by the product of the single-particle Gaussian wave packet as

$$\Phi_\alpha(\nu, R_i, \Lambda) = \phi_1^\nu(\uparrow, p)\phi_2^\nu(\downarrow, p)\phi_3^\nu(\uparrow, n)\phi_4^\nu(\downarrow, n) \tag{2}$$

with a single-nucleon Gaussian wave packet with spin $\chi_s$ ($s = \uparrow$ or $\downarrow$) and isospin $\eta_t$ ($t = p$ or $n$) wave functions

$$\phi_j^\nu(s, t) = \left(\frac{2\nu}{\pi}\right)^{3/4} \exp[-\nu(\boldsymbol{r}_j - \boldsymbol{\zeta}_i)^2]\chi_s\eta_t, \tag{3}$$

where

$$\boldsymbol{\zeta}_i = \boldsymbol{R}_i + i\Lambda \boldsymbol{e}^{\text{spin}} \times \boldsymbol{R}_i \tag{4}$$

with $\boldsymbol{e}^{\text{spin}}$ being a unit vector for the intrinsic-spin orientation of a nucleon. Apparently, $\Lambda = 0$ leads to the ordinary Brink-type $\alpha$-cluster basis function [2]. This multi-$\alpha$-cluster basis function can also describe the shell-model configuration. A limit of $d \to 0$ leads to the SU(3) limit of the shell-model configuration, $(0s)^4(0p)^8$ and $(0s)^4(0p)^{12}$ for $^{12}$C and $^{16}$O, respectively. The $\Lambda$ value controls the degree of the breaking of the $\alpha$ particles. As was shown in Ref. [21], the $j$-$j$ coupling shell-model closure configuration for $^{12}$C, $(0s_{1/2})^4(0p_{3/2})^8$, can be expressed by taking $\Lambda = 1$ with $d \to 0$.

Once the parameters of the trial function, i.e., $\nu$, $d$, and $\Lambda$, are set, it is straightforward to evaluate the one-body density distribution by

$$\tilde{\rho}(\boldsymbol{r}) = \langle\Phi|\sum_{i=1}^{A}\delta(\boldsymbol{r}_i - \boldsymbol{r})|\Phi\rangle/\langle\Phi|\Phi\rangle, \tag{5}$$

where $A$ is the mass number. Note $\sum_{i=1}^{A}\langle\boldsymbol{r}_i\rangle = 0$. As the wave function is expressed by a Slater determinant, this density distribution, in general, includes the center-of-mass motion, which crucially affects the density profiles in such light nuclei. Since the present wave function can be deduced to the product of the intrinsic and center-of-mass parts, the center-of-mass wave function can exactly be factored out by using a Fourier transform as [32]

$$\int d\boldsymbol{r}\, e^{i\boldsymbol{k}\cdot\boldsymbol{r}}\rho_{\text{int}}(\boldsymbol{r}) = \exp\left(\frac{k^2}{8A\nu}\right)\int d\boldsymbol{r}\, e^{i\boldsymbol{k}\cdot\boldsymbol{r}}\tilde{\rho}(\boldsymbol{r}). \tag{6}$$

The density distribution in the laboratory frame is finally obtained by averaging that center-of-mass-free intrinsic density distribution over angles as [33]

$$\rho(r) = \frac{1}{4\pi}\int d\hat{\boldsymbol{r}}\,\rho_{\text{int}}(\boldsymbol{r}). \tag{7}$$

The proton-nucleus elastic scattering cross sections are evaluated by using the Glauber model [34]. With the help of the optical limit approximation [34,35], the inputs to the theory are the density distribution obtained by Eq. (7) and the profile function, which describes the nucleon-nucleon scattering properties [36]. The elastic Coulomb phase is included in the calculation. The validity of the model is well tested, which can be seen in Refs. [37,38]. For more details, see, for example, Ref. [39] and references therein, showing the most recent application of this model.

To obtain the shell and cluster density profiles, we extend the prescription given in Ref. [39] and adapt it to the present multi-$\alpha$ cases. For the shell-model density profile (S-type), we take a small $\alpha$-cluster distance $d = 0.01$ fm and $\Lambda = 1$, which gives shell-model configurations of $(0s_{1/2})^4(0p_{3/2})^8$ for $^{12}$C and $(0s_{1/2})^4(0p_{3/2})^8(0p_{1/2})^4$ for $^{16}$O. Note that in the $^{16}$O case the result does not depend on the choice of $\Lambda$ as the $p$ shell is completely filled. The remaining parameter $\nu$ is fixed so as to reproduce the charge radius [40].

For the $\alpha$-cluster density profiles (C-type), the $\nu$ value is taken commonly to reproduce the charge radius of $\alpha$ particle, $\nu = 0.2656$ fm$^{-2}$, and we fix the $d$ value to reproduce the charge radii of $^{12}$C or $^{16}$O, where they are assumed to have equilateral triangular and tetrahedron shapes, respectively. The $\Lambda$ value is set to zero.

It is known that $^{12}$C is a mixture of shell and cluster configurations [12,13,14]. To incorporate this mixture, we introduce the mixed configuration (M-type): We take $\Lambda = 0.2$ and $d = 2$ fm following the optimal parameters based on a variational calculation [31] and fix the $\nu$ value to reproduce the charge radius of $^{12}$C. For $^{16}$O, here we only investigate a simple four-$\alpha$ cluster state with $\Lambda = 0$ because the breaking effect of $\alpha$ clusters is rather limited as shown in a $^{12}\text{C} + \alpha$ model calculation [24]: The ground state of $^{16}$O is insensitive to the strength of the spin-orbit interaction because the additional four nucleons compensate the attractive effect of the spin-orbit interaction in $^{12}$C.

Table I lists the calculated profiles of these obtained trial states for $^{12}$C and $^{16}$O: The fixed parameter sets, the total harmonic oscillator quanta $\langle Q\rangle$, the expectation values of single-particle spin-orbit operators $\sum_{i=1}^{A}\boldsymbol{l}_i\cdot\boldsymbol{s}_i$, $\langle LS\rangle$, single-particle parity operators $\sum_{i=1}^{A}P_i$ with $P_i f(\boldsymbol{r}_i) = f(-\boldsymbol{r}_i)$, $\langle P\rangle$. We see that the S-type states nicely reproduce the expected values of the ideal shell-model configurations, which are given in parentheses. In the C-type states, the cluster distance in $^{12}$C is significant and larger than the radius of $\alpha$ particle, 1.46 fm. The distance becomes larger for $^{16}$O, showing more developed $\alpha$-cluster structure.

TABLE I. Properties of the shell-model (S-type) and $\alpha$-cluster-model (C-type) trial states. Values in parentheses are obtained with the ideal shell-model configurations. The root-mean-square radii of $^{12}$C and $^{16}$O are adjusted to reproduce the experimental values 2.33 and 2.57 fm [40], respectively.

| | | $\nu$ (fm$^{-2}$) | $d$ (fm) | $\Lambda$ | $\langle Q\rangle$ | $\langle LS\rangle$ | $\langle P\rangle$ |
|---|---|---|---|---|---|---|---|
| $^{12}$C | S-type | 0.1886 | 0.010 | 1 | 8.0(8) | 4.0(4) | −4.0(−4) |
| | C-type | 0.2656 | 2.636 | 0 | 10.6 | 0.0(0) | −2.0 |
| | M-type | 0.2222 | 2.000 | 0.2 | 9.0 | 1.8 | −2.9 |
| $^{16}$O | S-type | 0.1635 | 0.010 | 1 | 12.0(12) | 0.0(0) | −8.0(−8) |
| | C-type | 0.2656 | 3.058 | 0 | 18.6 | 0.0(0) | −2.7 |

This characteristic is well reflected in the density profiles. Figure 1 plots those obtained one-body density distributions for $^{12}$C and $^{16}$O. The S-type and C-type exhibit quite different density profiles despite the fact that their root-mean-square radii are the same. In $^{12}$C, the C-type produces more depressed density distributions in the internal regions. This "bubble" structure comes from a well-developed $\alpha$ cluster configuration. Furthermore, this difference becomes more apparent in $^{16}$O, reflecting the larger $\alpha$ cluster distance than the C-type of $^{12}$C. In the surface regions, the C-type density distributions drop more rapidly than the S-type ones. Since the $\alpha$ particle has an extremely sharp nuclear surface, the C-type has a sharper surface than the S-type, reflecting the well-developed $\alpha$ cluster structure, i.e., the $\alpha$-$\alpha$ intercluster distance is large enough. As expected, the M-type gives the density distribution intermediate between the S-type and the C-type, as well as its properties, as shown in Table I.

To evaluate the density profiles near the nuclear surface more quantitatively, we also calculate the diffuseness parameter using the prescription given in Ref. [41]. By assuming a two-parameter Fermi (2pF) function as the one-body density distribution

$$\rho_{\rm 2pF}(\bar{R}, a, r) = \frac{\rho_0}{1+\exp[(r-\bar{R})/a]}, \tag{8}$$

the radius $\bar{R}$ and diffuseness $a$ parameters are determined by minimizing the value

$$\int_0^\infty dr\, r^2 |\rho_{\rm 2pF}(\bar{R}, a, r) - \rho(r)|. \tag{9}$$

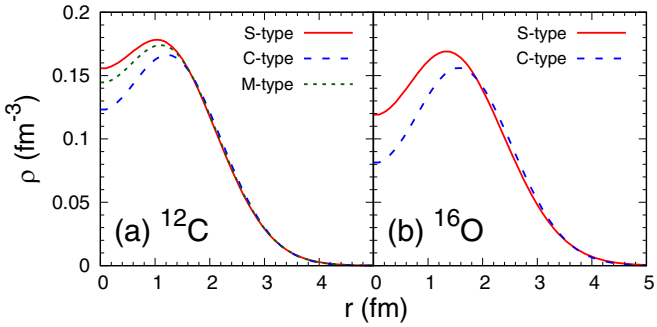


FIG. 1. One-body nucleon density distributions of (a) $^{12}$C and (b) $^{16}$O.

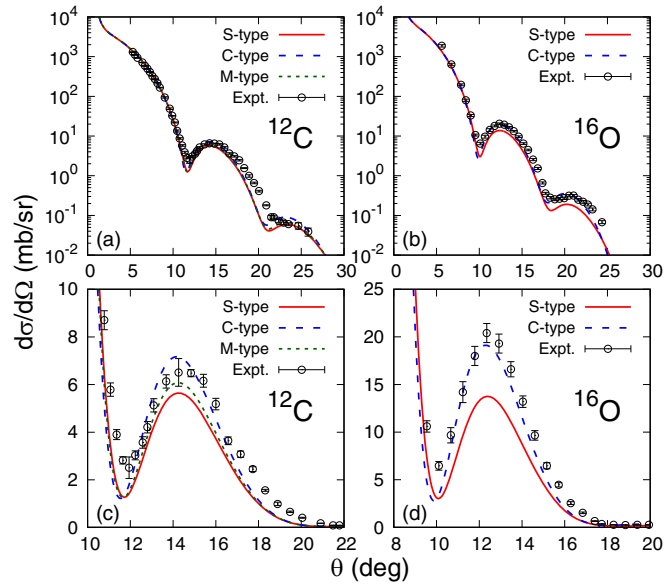


FIG. 2. Proton-nucleus differential elastic scattering cross sections for (a) $^{12}$C and (b) $^{16}$O at incident energies of 1000 MeV as a function of scattering angles. The cross sections in a linear scale around the first peak positions for (c) $^{12}$C and (d) $^{16}$O are also plotted for visibility. The experimental data are taken from Refs. [50,51].

$\rho_0$ is uniquely determined by the normalization condition. The extracted diffuseness parameters are 0.432 fm (0.401 fm) for the S-type (C-type) of $^{12}$C and 0.455 fm (0.405 fm) for the S-type (C-type) of $^{16}$O. We again confirm the sharper nuclear surfaces for the C-type quantitatively, and the difference between the S-type and the C-type are significant, which can be distinguished by the proton-nucleus elastic scattering experiment [41]. The diffuseness parameter for the M-type is found to be 0.423 fm, showing an intermediate value between the S-type and the C-type in $^{12}$C.

The difference in the surface density profile can be probed by the proton-nucleus elastic scattering [42]. Differential elastic scattering cross sections at around the first peak position reflects the surface density profiles and can be a promising probe to extract information on various nuclear structure [41,43–48]. Figure 2 plots the proton-nucleus differential elastic scattering cross sections for $^{12}$C and $^{16}$O. Incident energy is chosen to be 1000 MeV, where the experimental data are available both for $^{12}$C and $^{16}$O. The overall agreement between the theory and experiment is obtained. To see it more quantitatively, we also plot the cross sections around the first peak position in a linear scale as they are closely related to the density profiles near the nuclear surface. For $^{12}$C, the S-type underestimates the cross sections around the first peak, while the C-type is closer to the data even if it slightly overestimates. This suggests that the $^{12}$C wave function contains a significant amount of the $\alpha$-cluster component. In reality, the $^{12}$C wave function is the mixture of the shell and $\alpha$-cluster configurations as the M-type gives better reproduction of the data. For $^{16}$O, the theoretical cross sections with the C-type better reproduce the data, indicating more developed $\alpha$ cluster structure than $^{12}$C.

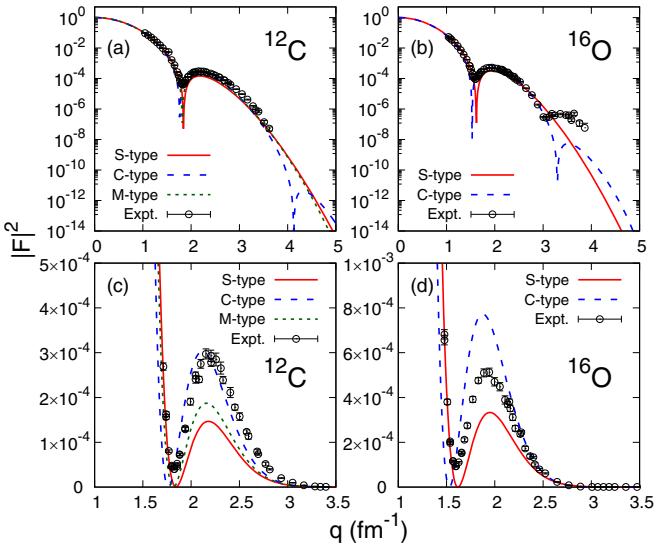


FIG. 3. Squared elastic charge form factors of $^{12}$C and $^{16}$O as a function of the momentum transfer. The experimental data are taken from Ref. [52].

The one-body density distributions have traditionally been investigated by electron scattering [49]. As it probes different parts of the density distribution, it is interesting to compare the elastic charge form factors obtained from the present trial states. The elastic charge form factor is evaluated by the Fourier transform of the density distribution with a finite size effect of a proton charge as [7]

$$|F(q)|^2 = \left| \frac{4\pi}{A} \int_0^\infty dr\, \rho(r) j_0(qr) r^2 \right|^2 \exp\left(-\frac{1}{2} a_p^2 q^2\right) \quad (10)$$

with $a_p^2 = 0.514$ fm$^2$, which reproduces the charge radius of a proton, 0.878 fm [40]. Figure 3 displays the square of the elastic charge form factors for $^{12}$C and $^{16}$O as a function of the momentum transfer $q$ both in logarithmic and linear scales. As already seen in the differential elastic scattering cross sections, a comparison with the experimental data supports a mixture of the shell and $\alpha$-cluster components both in $^{12}$C and $^{16}$O. The differences in the charge form factor become more evident at higher momentum transfer $q$. For $^{16}$O, no constraint is obtained in the present comparison of the data at $q \gtrsim 3\,\mathrm{fm}^{-1}$.

We confirmed a significant amount of $\alpha$-cluster components are included in the ground state wave functions in $^{12}$C and $^{16}$O. As seen in Fig. 1, the characteristics of the density profiles are not only for the surface region but also for internal regions. Since the electric force is much weaker than the nuclear force, the elastic charge form factor probes more internal regions than the proton-nucleus elastic scattering. Only the surface regions around the half density can be reflected [41,43] in the proton-nucleus elastic scattering. Though the sensitivity on the density profiles is different in proton or electron probes, we can see distinctive patterns enough to distinguish the shell and cluster configurations in the higher momentum transfer regions beyond the first peak. Such measurements up to the second peak could be useful for investigating both the surface and internal density profiles.

In summary, to settle the controversy on the dominance of the shell or cluster configurations, we have investigated the one-body density profiles of $^{12}$C and $^{16}$O using the basis states of the antisymmetrized quasicluster model, which can describe both the shell and $\alpha$-cluster configurations in a single scheme. These density profiles of the shell- and cluster-model type wave functions show quite different characteristics despite they reproduce the same charge radius. As the $\alpha$ cluster structure is developed, the density distribution exhibits sharper nuclear surface and more depressed central densities compared to the shell-model configuration.

We find, for the first time, that the evidence of the $\alpha$ clustering is imprinted on the one-body density profiles by comparing the proton-nucleus elastic scattering cross sections and the elastic charge form factors. The cross sections or charge form factors near the first peaks are significantly enhanced when the ground state wave function includes the $\alpha$ cluster component. The nuclear surface density profiles can be distinguished by measuring these quantities as a function of the momentum transfer up to the first peak position. It should be noted that the proton-nucleus scattering has the advantage that it can be more easily applied to unstable nuclei using inverse kinematics [53], though electron scattering for unstable nuclei is available [54]. Applications of the present method to heavier $4N$ systems as well as neutron-rich unstable nuclei surely help the universal understanding of the competition between the shell and cluster configurations.

This work was in part supported by JSPS KAKENHI Grants No. 18K03635, No. 22H01214, and No. 22K03618. We acknowledge the Collaborative Research Program 2022, Information Initiative Center, Hokkaido University.

[1] M. G. Mayer and H. G. Jensen, *Elementary Theory of Nuclear Shell Structure* (John Wiley & Sons, New York; Chapman & Hall, London, 1955).

[2] D. M. Brink, Many-Body Description of Nuclear Structure and Reactions, in *Proceedings of the International School of Physics "Enrico Fermi"*, Course XXXVI, edited by L. Bloch (Academic Press, New York, 1966), p. 247.

[3] N. Itagaki, S. Aoyama, S. Okabe, and K. Ikeda, Phys. Rev. C **70**, 054307 (2004).

[4] Y. Akaishi, M. Sakai, J. Hiura, and H. Tanaka, Prog. Theor. Phys. **51**, 13 (1974).

[5] C. Ishizuka, H. Takemoto, Y. Chiba, A. Ono, and N. Itagaki, Phys. Rev. C **105**, 064314 (2022).

[6] E. Uegaki, S. Okabe, Y. Abe, H. Tanaka, Prog. Theor. Phys. **57**, 1262 (1977).

[7] M. Kamimura, Nucl. Phys. A **351**, 456 (1981).
[8] P. Descouvemont, Phys. Rev. C **47**, 210 (1993).
[9] N. Itagaki, A. Ohnishi, and K. Kato, Prog. Theor. Phys. **94**, 1019 (1995).
[10] A. Tohsaki, H. Horiuchi, P. Schuck, and G. Röpke, Phys. Rev. Lett. **87**, 192501 (2001).
[11] A. Lovato, S. Gandolfi, R. Butler, J. Carlson, E. Lusk, S. C. Pieper, and R. Schiavilla, Phys. Rev. Lett. **111**, 092501 (2013).
[12] T. Otsuka, T. Abe, T. Yoshida, Y. Tsunoda, N. Shimizu, N. Itagaki, Y. Utsuno, J. Vary, P. Maris, and H. Ueno, Nat. Commun. **13**, 2234 (2022).
[13] Y. Kanada-En'yo, Prog. Theor. Phys. **117**, 655 (2007).
[14] M. Chernykh, H. Feldmeier, T. Neff, P. von Neumann-Cosel, and A. Richter, Phys. Rev. Lett. **98**, 032501 (2007).
[15] E. Epelbaum, H. Krebs, T. A. Lähde, D. Lee, Ulf-G. Meißner, and G. Rupak, Phys. Rev. Lett. **112**, 102501 (2014).
[16] E. E. Salpeter, Astrophys. J. **115**, 326 (1952).
[17] F. Hoyle, Astrophys. J. Suppl. Series **1**, 12 (1955).
[18] N. Itagaki, H. Masui, M. Ito, and S. Aoyama, Phys. Rev. C **71**, 064307 (2005).
[19] H. Masui and N. Itagaki, Phys. Rev. C **75**, 054309 (2007).
[20] T. Yoshida, N. Itagaki, and T. Otsuka, Phys. Rev. C **79**, 034308 (2009).
[21] N. Itagaki, J. Cseh, and M. Płoszajczak, Phys. Rev. C **83**, 014302 (2011).
[22] T. Suhara, N. Itagaki, J. Cseh, and M. Płoszajczak, Phys. Rev. C **87**, 054334 (2013).
[23] N. Itagaki, H. Matsuno, and T. Suhara, Prog. Theor. Exp. Phys. **2016**, 093D01 (2016).
[24] H. Matsuno, N. Itagaki, T. Ichikawa, Y. Yoshida, and Y. Kanada-En'yo, Prog. Theor. Exp. Phys. **2017**, 063D01 (2017).
[25] H. Matsuno and N. Itagaki, Prog. Theor. Exp. Phys. **2017**, 123D05 (2017).
[26] N. Itagaki, Phys. Rev. C **94**, 064324 (2016).
[27] N. Itagaki and A. Tohsaki, Phys. Rev. C **97**, 014307 (2018).
[28] N. Itagaki, H. Matsuno, and A. Tohsaki, Phys. Rev. C **98**, 044306 (2018).
[29] N. Itagaki, A. V. Afanasjev, and D. Ray, Phys. Rev. C **101**, 034304 (2020).
[30] N. Itagaki, T. Fukui, J. Tanaka, and Y. Kikuchi, Phys. Rev. C **102**, 024332 (2020).
[31] N. Itagaki and T. Naito, Phys. Rev. C **103**, 044303 (2021).
[32] W. Horiuchi, Y. Suzuki, B. Abu-Ibrahim, and A. Kohama, Phys. Rev. C **75**, 044607 (2007); **76**, 039903(E) (2007).
[33] W. Horiuchi, T. Inakura, T. Nakatsukasa, and Y. Suzuki, Phys. Rev. C **86**, 024614 (2012).
[34] R. J. Glauber, in *Lectures in Theoretical Physics*, edited by W. E. Brittin and L. G. Dunham (Interscience, New York, 1959), Vol. 1, p. 315.
[35] Y. Suzuki, R. G. Lovas, K. Yabana, and K. Varga, *Structure and Reactions of Light Exotic Nuclei* (Taylor & Francis, London, 2003).
[36] B. Abu-Ibrahim, W. Horiuchi, A. Kohama, and Y. Suzuki, Phys. Rev. C **77**, 034607 (2008); **80**, 029903(E) (2009); **81**, 019901(E) (2010).
[37] W. Horiuchi, S. Hatakeyama, S. Ebata, and Y. Suzuki, Phys. Rev. C **93**, 044611 (2016).
[38] S. Hatakeyama and W. Horiuchi, Nucl. Phys. A **985**, 20 (2019).
[39] W. Horiuchi and N. Itagaki, Phys. Rev. C **106**, 044330 (2022).
[40] I. Angeli and K. P. Marinova, At. Data Nucl. Data Tables **99**, 69 (2013).
[41] S. Hatakeyama, W. Horiuchi, and A. Kohama, Phys. Rev. C **97**, 054607 (2018).
[42] H. Sakaguchi and J. Zenihiro, Prog. Part. Nucl. Phys. **97**, 1 (2017), and references therein.
[43] V. Choudhary, W. Horiuchi, M. Kimura, and R. Chatterjee, Phys. Rev. C **102**, 034619 (2020).
[44] V. Choudhary, W. Horiuchi, M. Kimura, and R. Chatterjee, Phys. Rev. C **104**, 054313 (2021).
[45] W. Horiuchi, T. Inakura, and S. Michimasa, Phys. Rev. C **105**, 014316 (2022).
[46] M. Tanaka, M. Takechi, M. Fukuda, D. Nishimura, T. Suzuki, Y. Tanaka, T. Moriguchi, D. S. Ahn, A. Aimaganbetov, M. Amano *et al.*, Phys. Rev. Lett. **124**, 102501 (2020).
[47] W. Horiuchi, Prog. Theor. Exp. Phys. **2021**, 123D01 (2021).
[48] W. Horiuchi and T. Inakura, Phys. Rev. C **105**, 044303 (2022).
[49] R. Hofstadter, Rev. Mod. Phys. **28**, 214 (1956).
[50] G. D. Alkhazov, G. M. Amalsky, S. L. Belostotsky, O. A. Domchenkov, Yu. V. Dotsenko, and V. E. Starodubsky, Phys. Lett. B **42**, 121 (1972).
[51] G. D. Alkhazov, S. L. Belostotsky, A. A. Vorobyov, O. A. Domchenkov, Yu. V. Dotsenko, N. P. Kuropatkin, and V. N. Nikulin, Yad. Fiz. **42**, 8 (1985).
[52] I. Sick and J. S. McCarthy, Nucl. Phys. A **150**, 631 (1970).
[53] Y. Matsuda, H. Sakaguchi, H. Takeda, S. Terashima, J. Zenihiro, T. Kobayashi, T. Murakami, Y. Iwao, T. Ichihara, T. Suda *et al.*, Phys. Rev. C **87**, 034614 (2013).
[54] K. Tsukada, A. Enokizono, T. Ohnishi, K. Adachi, T. Fujita, M. Hara, M. Hori, T. Hori, S. Ichikawa, K. Kurita *et al.*, Phys. Rev. Lett. **118**, 262501 (2017).